THE RECOVERY OF THE OPTIMAL DAMPING CONSTANT BY THE MRF DAMPER

Gabriele Barbaraci*[1]*, Gabriele Virzi' Mariotti

UDC: 62-272.8:536.5
629.011.85

INTRODUCTION

Real-time damping control of automotive suspension systems can reduce the low frequency vehicle body motions while enhancing the vehicle road holding characteristics. Other benefits of semi-active suspension systems having controllable damping are: reduced hardness from high frequency road disturbances (for a smoother ride) and better handling during transient maneuvers. The work presented in this paper was carried out with the purpose of making a theoretical study of the dynamic behavior of a 2DOF system using smart fluids [1]-[2] called Magneto-Rheological (MR). We considered the MR fluids which produce superior effects at voltages well below 12V and hence are more preferable for automotive use then the ER fluids which require very high electrical fields (on the order of 5kV/mm) to produce the desired effects. The Magneto-Rheological (MR) fluids are a class of controllable fluids having micrometer-sized magnetizable solids dispersed in a non-magnetic fluid such as synthetic mineral oil. The MR fluids are freely flowing in the absence of a magnetic field but they are changing into a paste-like substance in the presence of a magnetic field in a quick and completely reversible manner. The yield strength of a MR fluid can be continuously controlled by the applied magnetic field with response times in the range of milliseconds. This feature paved the way for the MR fluids as simple interfaces between mechanical systems and electronic controllers for fast, controllable actuators having valves without moving parts, especially in controllable dampers used in detail in the Magnetic Ride Control system.

2. MATHEMATICAL MODEL

Figure 1 shows a sketch of a 2DOF system used for this study

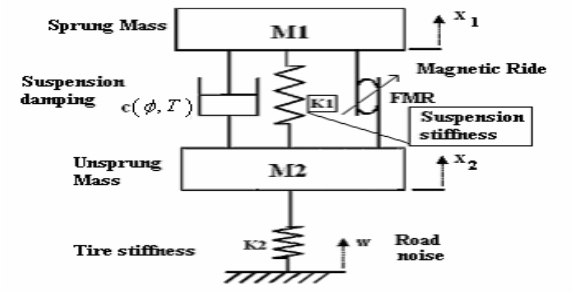

Figure 1: *A schematic view of a shock absorber for a 2DOF system*

[1] Corresponding author e-mail: barbaraci@dima.unipa.it , Universitè di Palermo, Dipartimento di Meccanica, Viale delle Scienze, 90128 Palermo, Italy

What is established due to the displacement along a positive direction x_1 is the sum of a reaction force acting in the sprung mass according to which it has its motion equation (1).

$$m_1\ddot{x}_1(t)+c(\phi,T)\dot{x}_1(t)+k_1x_1(t)-c(\phi,T)\dot{x}_2(t)-k_1x_2(t)-F_{MR}=0 \quad (1)$$

The same procedure is applied to the unsprung mass owing to which it has (2)

$$m_2\ddot{x}_2(t)+c(\phi,T)\dot{x}_2(t)+k_1x_2(t)-c(\phi,T)\dot{x}_1(t)-k_1x_1(t)-k_2y(t)+F_{MR}=0 \quad (2)$$

where $c(\phi,T)$ represents the damping constant varying with temperature and iron fraction particle volume of a fluid.
Both equations are shown in the following matrix form (3):

$$\mathbf{M}\ddot{\mathbf{q}}(t)+\mathbf{C}(\phi,T)\dot{\mathbf{q}}(t)+\mathbf{K}\mathbf{q}(t)+\mathbf{b}F_{MR}+\mathbf{g}w(t)=\mathbf{0} \quad (3)$$

where

$$\mathbf{M}=\begin{bmatrix} m_1 & 0 \\ 0 & m_2 \end{bmatrix};\ \mathbf{C}(\phi,T)=\begin{bmatrix} c(\phi,T) & -c(\phi,T) \\ -c(\phi,T) & c(\phi,T) \end{bmatrix};\ \mathbf{K}=\begin{bmatrix} k_1 & -k_1 \\ -k_1 & k_1+k_2 \end{bmatrix};\ \mathbf{b}=\begin{bmatrix} 1 \\ -1 \end{bmatrix};\ \mathbf{g}=\begin{bmatrix} 0 \\ -k_2 \end{bmatrix}$$

$$\mathbf{q}(t)=\begin{bmatrix} x_1(t) & x_2(t) \end{bmatrix}^T$$

Carrying out a change of the variable we put:

$$\begin{cases} \mathbf{z_1}(t)=\mathbf{q}(t) \\ \mathbf{z_2}(t)=\dot{\mathbf{q}}(t) \end{cases} \Rightarrow \dot{\mathbf{z}}_\mathbf{1}(t)=\mathbf{I}\ \mathbf{z_2}(t)/\mathbf{I}$$

in order to obtain the state space model (4):

$$\dot{\mathbf{z}}(t)=\mathbf{A}\mathbf{z}(t)+\mathbf{b_z}F_{MR}+\mathbf{g_z}w(t) \quad (4)$$

where

$$A=\begin{bmatrix} 0 & I \\ -M^{-1}K & -M^{-1}C(T) \end{bmatrix};\quad b_z=\begin{bmatrix} 0 \\ -M^{-1}b \end{bmatrix};\quad g_z=\begin{bmatrix} 0 \\ -M^{-1}g \end{bmatrix}$$

3. ACTUATOR

The figure 2 shows the cross section of the comprehensive electromagnet coil in the hypothesis that this last one has a square section.

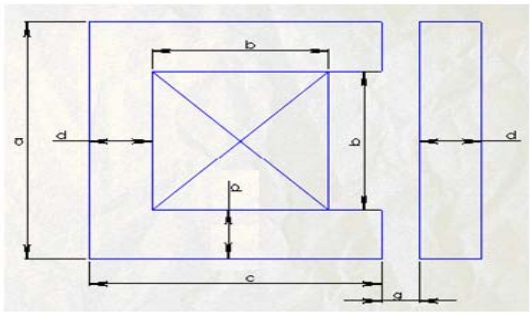

Figure 2: *A cross of the section of actuator and coil*

The mechatronic system that allows generating a damping force varying of the magnetic field at first depends on the circulation ampere's law (5):

$$N\ I = H_0 l_0 + \sum_i H_i l_i = \Phi\left(\frac{2l_0}{\mu_0 S_0} + \sum_i \frac{l_i}{\mu_r S_i}\right) \tag{5}$$

where l_0 and l_i are the length of a circulation in the gap and the iron space respectively, while S_0 e S_i are the cross section of the magnetic flow which in this case is the same as in the empty space or as in the iron one because of a small gap.
Since the reluctance in the iron is negligible with regard to the empty one ($\mu_r \ll \mu_0$) [3]-[4], we considered only the addend of the second member shown in an integral form such as (6), [5]:

$$\int \vec{H} \cdot \hat{n}\, dl = \int \vec{J} \cdot \hat{n}\, dA_C \tag{6}$$

where A_C is the coil cross section. The last step to carry out is to calculate the cross section of the polar expansion relative to the electromagnet. The realized magnetic field $\vec{B}$ obviously depends on the induction magnetic field $\vec{H}$ through the iron fraction particle volume of a fluid, [6]:

$$B(H) = 1.91 \cdot \phi^{1.133} \cdot \left[1 - e^{-10.97 \cdot \mu_0 \cdot H}\right] + \mu_0 \cdot H \tag{7}$$

the pathway of which is calculated by varying the iron particle fraction and induction magnetic field as shown in the figure 3.

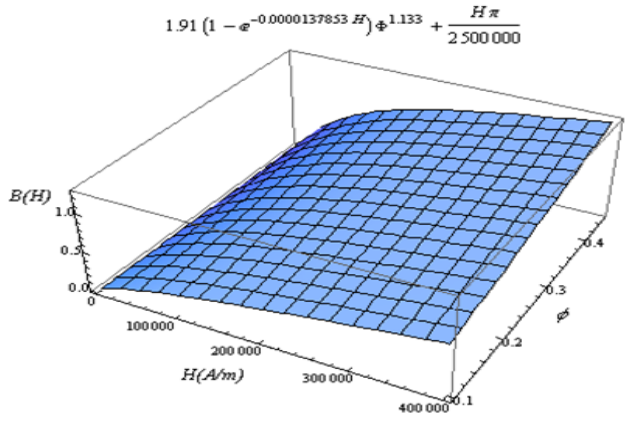

Figure 3: *A magnetic field B versus* ϕ and H

As we can see from the figure 3, the magnetic field increases with the increase of ϕ and of the induction magnetic field H as well. The yield strength equation (8), [6]:

$$Y_s = C_f \cdot 271700 \cdot \phi^{1.5239} \cdot Tanh\left(6.33 \times 10^{-6} \cdot H\right) \tag{8}$$

assumes the same behavior although what must be taken into account is another parameter called a carrier fluid constant C_f [6]. The figures 4 and 5 show the pathway of the yield strength varying with the magnetic field *H* in the two distinguished cases.

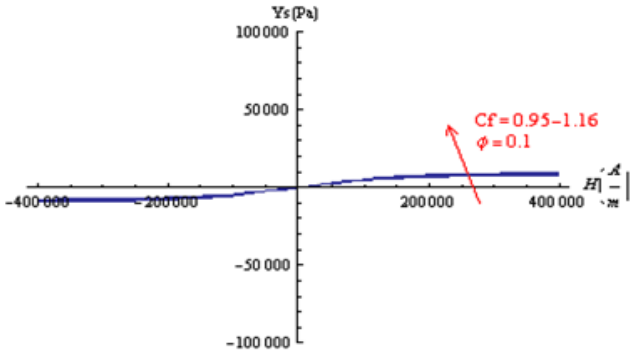

Figure 4: *The yield strength versus H varying carrier fluid constant* C_f *and fixed* $\phi = 0.1$.

What is shown in the figure 4 is the variation with the carrier fluid constant at $\phi = 10\%$. A small variation of $Y_S\left(C_f, H\right)\Big|_{\varphi=10\%}$ can be seen there with regard to $Y_S\left(\phi, H\right)\Big|_{C_f=0.95}$ whose data are plotted in the figure 5.

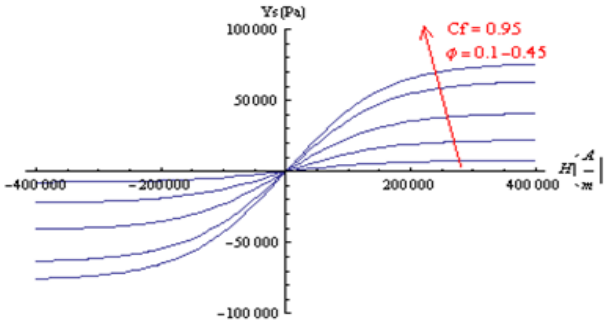

Figure 5: The yield strength versus *H* varying the carrier fluid constant ϕ and fixed $C_f = 0.95$

A similar behavior has $c(\phi,T)$ whereas ϕ and temperature *T* are changing. It depends on the dynamic viscosity as it is shown in (8), [7]:

$$\eta(\phi,T)=\eta_0\left(1-\frac{\phi}{\phi_{\max}}\right)^{-k\,\phi_{\max}} e^{\left[-\alpha(T-40)\right]} \tag{8}$$

whose a 3D plot is shown in the figure (6). We can see that $\eta(\phi,T)$ decreases with the increase of the temperature and while it increases with the increase of ϕ once *T* is fixed. In this application we fixed the iron fraction particle volume at the value $\bar{\phi}=0.4$ in order to have $\eta(\bar{\phi},T)$ as it is shown in the figure (7):

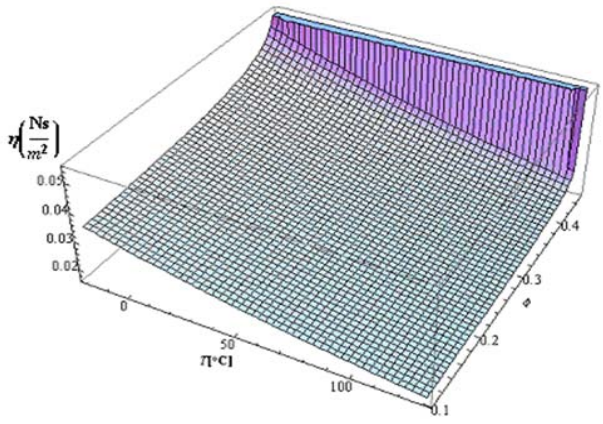

Figure 6: The dynamic viscosity η versus ϕ and T .

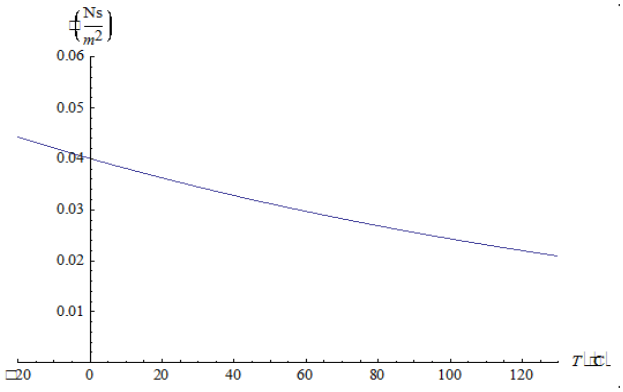

Figure 7: *The dynamic viscosity* $\eta(\bar{\phi},T)$ *versus* T

The equations (9), (10), (11) and (12) are the electromechanical relations through which the proportions of the magnetorheological damper have been determined. The force generated from the passive system turns out from the expression (9) from which the damping constant is extrapolated (10) and where V represents the relative speed between the sprung and unsprung mass, while (11) is the one relative to the MRF. The following represents the coil cross section whose axial dimension is equal to the square root of (12):

$$F_{pass}\left(V_d\right)=\left(\frac{6\,\eta\left(\bar{\phi},\bar{T}\right)\,a}{\pi r_m g^3}\right)\left(\pi r_{piston}^2-\pi r_{rod}^2\right)^2 V \tag{9}$$

$$c\left(\bar{\phi},\bar{T}\right)\Big|_{\substack{\bar{T}=40°C\\ \bar{\phi}=0.4}}=\left(\frac{6\,\eta\left(\bar{\phi},\bar{T}\right)\,a}{\pi r_m g^3}\right)\left(\pi r_{piston}^2-\pi r_{rod}^2\right)^2=\text{optimal damping constant} \tag{10}$$

$$F_y\left(H\right)=Y_s 2S_0=Y_s\left[2d\left(2\pi r_{piston}\right)\right] \tag{11}$$

$$A_C=\frac{H2g}{f_c J} \tag{12}$$

A short parenthesis must be opened for the meaning of the optimal damping constant. This term refers to the damping constant that must be realized at the minimum of the maximum acceleration of a system during its oscillation. It is equal to $c\left(\bar{\phi},\bar{T}\right)\Big|_{\substack{\bar{T}=40°C\\ \bar{\phi}=0.4}}=\sqrt{\frac{m_2\left(\frac{k_1k_2}{k_1+k_2}\right)}{2}}$ according to which the dynamic behavior response is characterized in a transient condition [8].

The cross section of the coil has been chosen in correspondence to the point of maximum magnetic permeability whereas this value is the one corresponding to the error of 10% between the linear and real pathway of the first magnetization curve. What has been said is on the Table 1 which leads to the Table 2 regarding the geometry of the electromagnet.

Table 1: *Initial data for electromagnet design*

Symbol	Quantity	Values (SI)
r_p	piston radius	0.03 m
r_r	rod radius	0.004 m
r_m	mean radius	0.017 m
A_p	piston area	0.0028 m^2
A_r	rod area	5×10^{-5} m^2
L_g	gap	1×10^{-3} m
$\bar{T}$	design temperature	+40 °C
k	Intrinsic viscosity	0.2750 Ns/m^2
η_0	dynamic viscosity at design temperature	0.0251 Ns/m^2
$\bar{\phi}$	design fraction volume of iron particles	40 %
ϕ_{max}	maximum fraction volume of iron particles	0.45 %
α	temperature coefficient	0.005 $°C^{-1}$
F_{yield}	design yield stress force in linearity range	100 N
C_f	carrier fluid costant	0.95
$c\left(\bar{\phi},\bar{T}\right)$	optimal damping costant	1000 N s/m
H	magnetic field	17840 A/m
J	density current	10^6 A/m^2
f_c	copper winding factor	50 %

Table 2: *Final data for electromagnet design*

Symbol	Quantity	Values (SI)
τ_{yield}	yield stress	7184 N
d	pole thickness	0.037 m
$A_{pole}(2S_0)$	pole expansion surface	0.014 m^2
a	piston axial dimension	0.0352 m
A_c	coil cross section	$7.13\times10^{-5}m^2$
b	Axial dimension of coil winding	0.0084 m

Once the data showed in the Table 2 are obtained, we have analyzed the plot of $C_d = c\left(\bar{\phi}, T\right)\Big|_{\bar{\phi}=0.4}$ varying with temperature as it is shown in the figure (8):

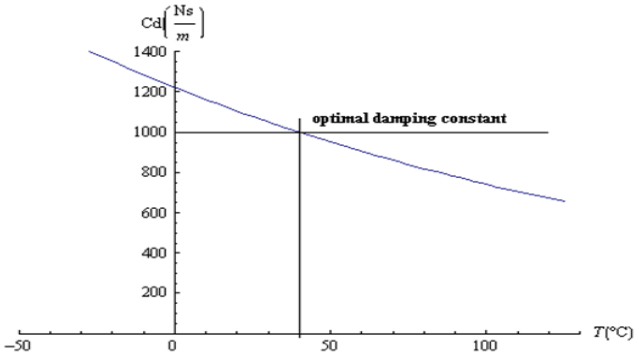

Figure 8: The damping constant C_d versus T once fixed $\bar{\phi} = 0.4$ with the optimal one which is shown as well

The figure (9) shows that $c\left(\bar{\phi}, T\right)\Big|_{\bar{\phi}=0.4}$ has a similar pathway of dynamic viscosity. This leads to a different dynamic behavior of the system varying with temperature. What has been said before is shown by plotting the real and imaginary part of eigenvalues produced by the dynamic matrix **A** of the system (4) varying the temperature in a range $-20 \le T \le 130\ °C$.

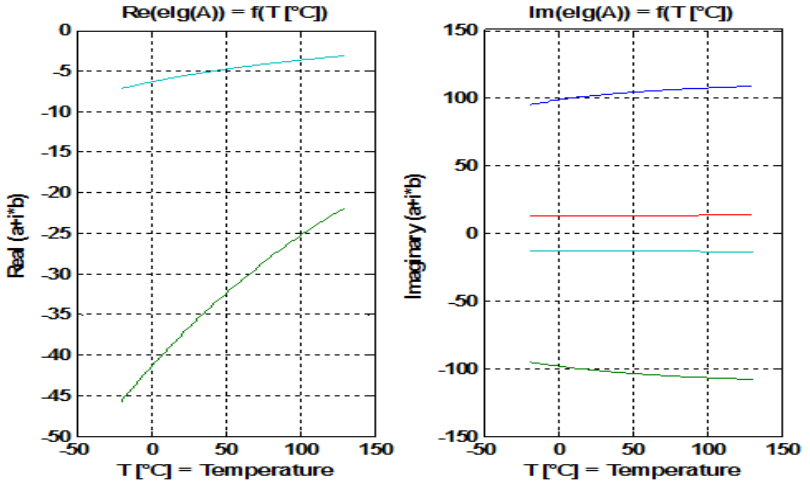

Figure 9: *The real and imaginary part of eigenvalues of the dynamic system varying with temperature*

We asked ourselves if the introduction of the MRF technology could recover the optimal damping constant varying with temperature. We know that in the optimal conditions and without the introduction of the MRF force, the expression of the force turns out from (13):

$$F_{tot(opt.)} = F_{pass.(opt.)}\left(\bar{\phi},\bar{T}\right) = c\left(\bar{\phi},\bar{T}\right)\Big|_{\substack{\bar{T}=40°C \\ \bar{\phi}=0.4}} \cdot V \tag{13}$$

If we assume an increase of the temperature beginning from $T = 40\,°C$ then the damping constant will decrease from the optimal value. Since the presence of the MRF involves an increase of the fluid viscosity, we can compensate the loss of a damping effect by means of the induction magnetic field *H* in the range $T > 40\,°C$.

Because of the presence of the magnetorheological fluid, this contribution must be added to the (13) in order to obtain (14), so that the same reaction force could be realized in the optimal conditions.

$$F_{tot(opt.)} = F_{MRF}\left(\bar{\phi},H\right) + F_{pass.}\left(\bar{\phi},T\right) \tag{14}$$

where

$$F_{MRF}\left(\bar{\phi},H\right) = C_f \cdot 271700 \cdot \bar{\phi}^{1.5239} \cdot A_{pole} \cdot \tanh\left(6.33\times10^{-6}\cdot H\right) \tag{15}$$

$$F_{pass.}\left(\bar{\phi},T\right) = c\left(\bar{\phi},T\right)\cdot V \tag{16}$$

From (14) we obtain the expression of the magnetic field $\vec{H}$ inorder to compensate decreasing of the damping constant, taking into account that with the increase of the temperature (14) must be verified.

By manipulating (14), (15), and (16) the value of the magnetic field is obtained (17):

$$H\left(T,V\right) = \frac{1}{6.33\times10^{-6}} \cdot \arctan^{-1}\left[\left(\frac{c\left(\bar{\phi},\bar{T}\right)\Big|_{\substack{\bar{T}=40°C \\ \bar{\phi}=0.4}} - c\left(\bar{\phi},T\right)}{\beta\left(C_f,\bar{\phi},A_p\right)}\right)\cdot V\right] \tag{17}$$

in order to induce a recovery of the optimal damping constant during the increase of the temperature ranging from $T > 40\,°C$ as a state feedback of the reduced order (in the sense that only the speed value is considered whereas the state vector contains displacements as well) such as to provide a time variant control signal with temperature.

The expression of the force generated to do what has been said so far (18):

$$F_{tot(opt.)} = \beta\left(C_f, \bar{\phi}, A_p\right) \cdot \tanh\left(6.33 \times 10^{-6} \cdot H\left(T,V\right)\right) + c\left(\bar{\phi}, T\right) \cdot V \tag{18}$$

where

$$\beta\left(C_f, \bar{\phi}, A_p\right) = C_f \cdot 271700 \cdot \bar{\phi}^{1.5239} \cdot A_{pole} \tag{19}$$

The magnetic field which provides the results presented above is dependent on the relative speed value of the unsprung mass with the once fixed temperature, as it is shown in the figure 10:

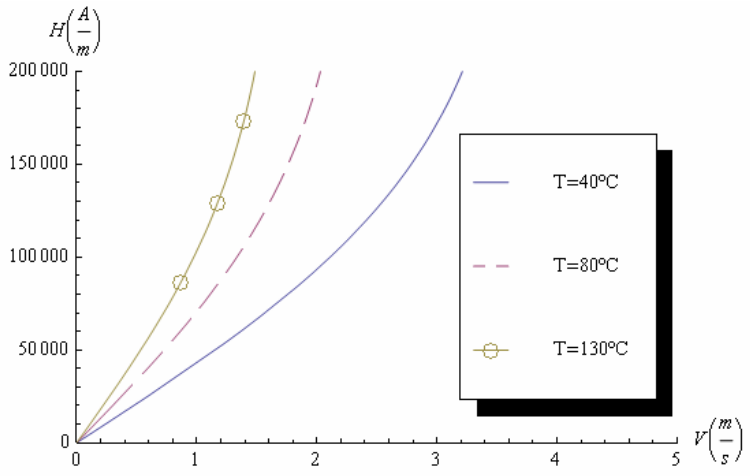

Figure10: *The force generated by the MRF to recover the optimal damping constant varying with temperature*

Once the temperature is fixed, as it is shown in the figure 10, we can see how to realize the compensation effect in order to recover the optimal damping constant. The electromagnets have to produce a magnetic induction field increasing the speed of the unsprung mass. This is a great problem because of the thermal limitation due to the copper wire whose electromagnets are built up. In fact, what we can also see from the figure is that, at very small speed, the value corresponds to the high induction magnetic field. However, if a

compensation effect was feasible we would obtain a constant dynamic behavior varying with temperature.

The compensation of the optimal damping constant leads the system to have the same dynamic behavior varying with temperature as we can see from the plotting of the real and imaginary part of eigenvalues,as it is shown in the figure 11.

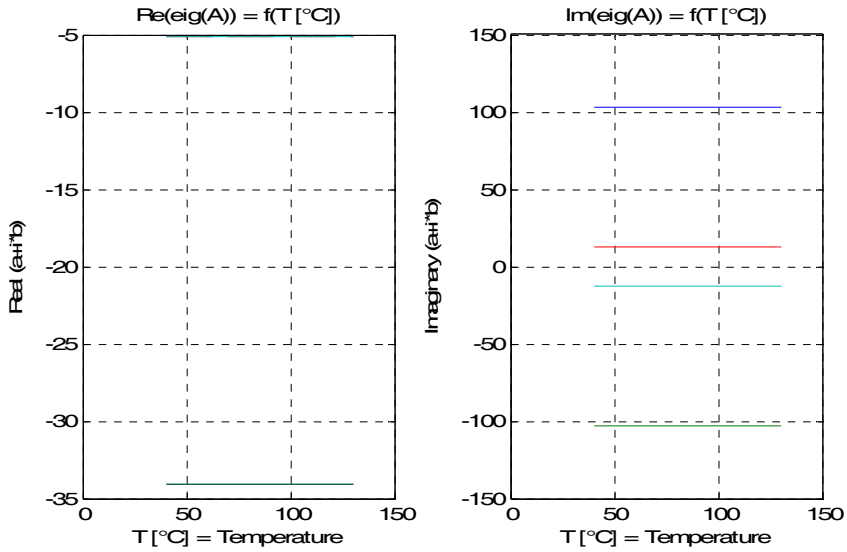

Figure 11: *The real and imaginary part of eigenvalues of a dynamic system with the MRF varying with temperature*

As we can see from the figure 11 the real and imaginary part of eigenvalues of the system are constant. This means that the equations of motion are characterized by the same linear combination of natural vibration varying with temperature for $T > 40\,°C$.

4. SIMULATIONS AND RESULTS

All simulations were performed by Simulink, a package of MATLAB. The figure (12) shows the block scheme through which simulations were performed while varying with temperature. Each block contains a sub-block, as it is shown in the figure (13), in which there is the dynamic system presented.

In this case they are considered within the blocks at $T = 40\,°C, T = 80\,°C,$ and $T = 130\,°C$ as a specified range of the temperature where the compensation is possible for our study. By simulating the system with a step input with the amplitude of $n = 0.02m$ at $\bar{t} = 2s$ in a simulation for $t \in [0,4]s$, see the figure (13-left), we can see that the overshoot increases by increasing of temperature, see the figure (13-right). This leads to a general modification of transient response in terms of settling times.

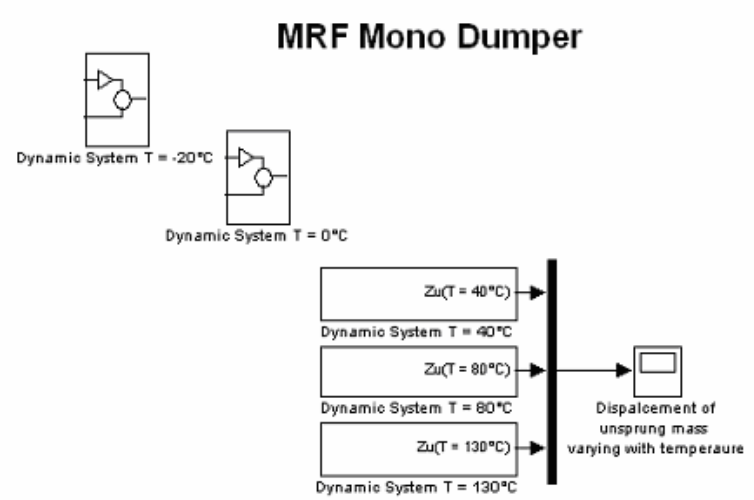

Figure 12: *A block scheme of the dynamic system with the MRF varying with temperature*

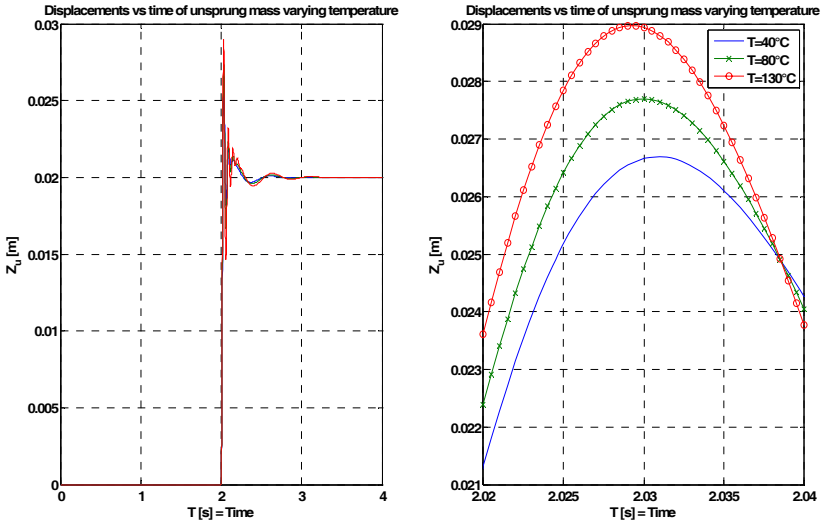

Figure 13: *Displacements of the unsprung mass without MRF varying with temperature*

By the introduction of MRF technology for example in the system having temperature $T = 80\,°C$, there is a small variation in a dynamic behavior. The figure (14-left) shows a simulation during which the system is analyzed in the case it has a temperature $T = 40\,°C, T = 80\,°C,$ and $T = 80\,°C$ with the MRF compensation. From the figure 14-right we can see how the introduction of the compensation effect reduces the overshoot

corresponding to the simulation at $T = 80\,°C$ well below than the one at temperature $T = 40\,°C$

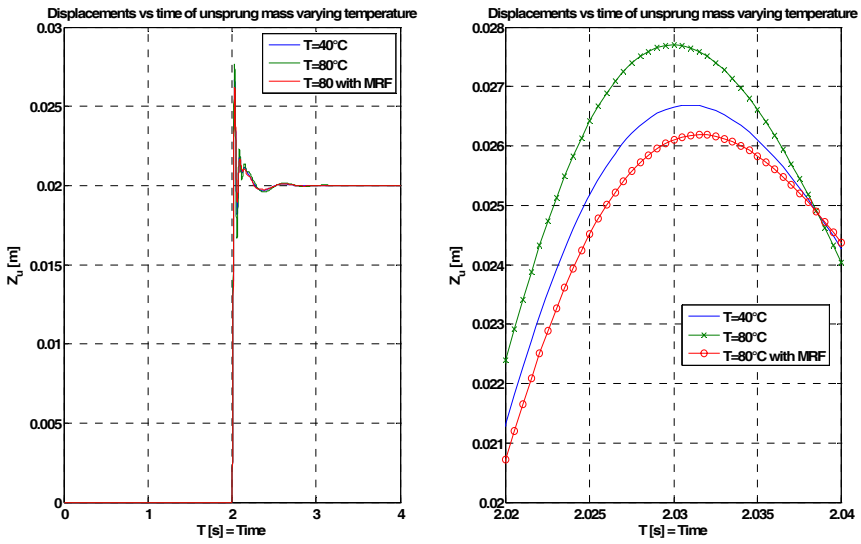

Figure 14: *Displacements of the unsprung mass with the MRF compensation varying with temperature*

5. CONCLUSIONS

After a short introduction to magnetorheological fluids and their advantages as for the power supplied with regard to the electrorheological ones, we have analyzed the behavior of the magnetic field $\vec{B}\left(\vec{H},\phi\right)$ and $Y_S\left(\text{yield strength}\right)$ whereas $Y_S\left(\phi,H\right)\big|_{C_f=0.95}$ makes higher contributions than $Y_S\left(C_f,H\right)\big|_{\varphi=10\%}$. According to the analysis of dynamic viscosity, which decreases with the increase of the temperature, it was seen that the optimal damping constant is not held in such a manner to induce a higher oscillation of the unsprung mass in transient response. The oscillations are characterized by the overshoot which increases with the increase of the temperature because of decreasing of the damping constant. We have also seen that in the case of the real yield strength expression, obtaining a gain as independent on the unsprung mass speed is not feasible. However, if a nonlinear expression is used, there would be a great value of the induction magnetic field in a range of

the speed where another contribution to the increase of the temperature is a joule dissipation effect. This leads to a higher and more complicated design of the electromagnet because it has to support high values of the induction magnetic field and produce low dissipation of thermal energy.

Moreover, decreasing of the damping constant was compensated by the introduction of a magnetic field whose value was considered in a range of a linear response of the yield strength produced by the actuator in order to obtain an equivalent damping constant $c_H\left(\bar{\phi},T\right)$. This constant represents a gain to generate a control signal by a state feedback of a reduced order which can maintain the same transient response within a range of the unsprung mass speed with the once fixed temperature. The future development will deal with the influence of this study upon the lateral dynamic behavior due to the force developed in a full car during turning and maneuvering whereas the centrifugal force produces such a virtual increasing and decreasing of the sprung mass to modify the optimal damping constant for the inner and outside part of a vehicle respectively.

LIST OF SYMBOLS

m_1	Sprung mass
m_2	Unsprung mass
x_1	Degree of freedom of the sprung mass
x_2	Degree of freedom of the unsprung mass
w	Road noise pattern
k_1	Suspension stiffness
k_2	Tire stiffness
T	Temperature
$c\left(\phi,T\right)$	Suspension dumping versus temperature
F_{MR}	Magnetic-Ride force
ϕ	Fraction volume of iron particles
$\phi_{\max}$	Max fraction volume of iron particles
C_f	Carrier fluid constant
k	Intrinsic viscosity
a	Axial length of the electromagnet

L_g	gap
M	Mass matrix
$\mathbf{C}(\phi,T)$	Damping matrix
K	Stiffness matrix
A	Matrix of dynamic
b	Vector for the sign of F_{MR}
g	Noise tire stiffness vector

REFERENCES

[1] Rabinow, 'Magnetic-Fluid Control Devices', *SAE Quwlerly Trmsacrions* , Oct. 1949, pp.639-648.

[2] M.R. Jolly et al**,** *Properties and Applications of Commercial Magnetorheological Fluids*, SPIE 5th Annual Int. Symposium Structures and Materials, San Diego, CA, March 15, 1998. Hochschulverlag.

[3] G. Schweitzer, H. Bleuler, and A. Traxler, *Active Magnetic Bearings*. ETH Zürich: Vdf AG an der ETH Zürich, 1994.

[4] G. Barbaraci, G. V. Mariotti, 'AIAS Conference' *Controllo sub-ottimo per un albero rotante in levitazione magnetica attiva.* Torino 2009.

[5] G. Schweitzer. E. H. Maslen, *Magnetic Bearings: Theory, Design, and Application to Rotating Machinery*, Springer Editions. Zurich, 2009.

[6] Website Lord Corporation; www.lord.com.

[7] C. S. Namudur, M. A. Golden i, J. Praeckel, '*IEEE Xplore*' *Concurrent Research and Development of a Magnetic Ride Control System*, March2003, pp.2853-2855

[8] G. V. Mariotti, *Tecnica delle Costruzioni di Macchine*, Aracne Editions, September 2007, pp.16-18.